Journal of the Mechanics and Physics of Solids 61 (2013) 2588–2604

Contents lists available at ScienceDirect

Journal of the Mechanics and Physics of Solids

journal homepage: www.elsevier.com/locate/jmps

On the strain hardening and texture evolution in high manganese steels: Experiments and numerical investigation ☆

Yongqiang Li [a], Lianchun Zhu [a], Yao Liu [a], Yujie Wei [a,*], Yanxin Wu [b], Di Tang [b], Zhenli Mi [b,*]

[a] LNM, Institute of Mechanics, Chinese Academy of Sciences, Beijing 100190, PR China
[b] National Engineering Research Center for Advanced Rolling Technology, University of Science and Technology Beijing, Beijing 100083, PR China

ARTICLE INFO

Article history:
Received 2 August 2012
Received in revised form
17 July 2013
Accepted 7 August 2013
Available online 17 August 2013

Keywords:
Twinning induced plasticity
Deformation twinning
Strain hardening
Crystal plasticity
Finite-element analysis

ABSTRACT

We present a systematic investigation on the strain hardening and texture evolution in high manganese steels where twinning induced plasticity (TWIP) plays a significant role for the materials' plastic deformation. Motivated by the stress–strain behavior of typical TWIP steels with compositions of Fe, Mn, and C, we develop a mechanistic model to explain the strain-hardening in crystals where deformation twinning dominates the plastic deformation. The classical single crystal plasticity model accounting for both dislocation slip and deformation twinning are then employed to simulate the plastic deformation in polycrystalline TWIP steels. While only deformation twinning is activated for plasticity, the simulations with samples composed of voronoi grains cannot fully capture the texture evolution of the TWIP steel. By including both twinning deformation and dislocation slip, the model is able to capture both the stress–strain behaviors and the texture evolution in Fe–Mn–C TWIP steel in different boundary-value problems. Further analysis on the strain contributions by both mechanisms suggests that deformation twinning plays the dominant role at the initial stage of plasticity in TWIP steels, and dislocation slip becomes increasingly important at large strains.

1. Introduction

The high ultimate strength, combined with a high hardening modulus to resist deformation localization in the twinning induced plasticity (TWIP) steels, stimulate broad interests from both academic society and industries. For example, Fe–Mn–Si–Al and Fe–Mn–C austenitic TWIP steels have been proposed to many applications (Grässel et al., 2000) where high strength and/or light weight materials are desired for lower energy consumption and further enhancement in safety, which is of paramount importance in the automotive industry (Liu et al., 2012). For example, the ultimate strength over density ratio of TWIP steels is comparable to that of nanocrystalline magnesium (Wei and Anand, 2007). Typically, the 0.2% yield strengths of TWIP steels are in the range of 350–500 MPa, which are at the same level of several conventional high strength steels including dual-phase (DP) steels and transformation-induced plasticity (TRIP) steels (Bouaziz et al., 2011a, 2011b; Krauss, 1990; Yoo et al., 2009; Zavattieri et al., 2009). Following the initial yielding, TWIP steels harden at a nearly constant

* Corresponding authors.
E-mail addresses: yujie_wei@lnm.imech.ac.cn (Y. Wei), mizl@nercar.ustb.edu.cn (Z. Mi).

0022-5096/$ - see front matter © 2013 The Authors. Published by Elsevier Ltd. All rights reserved.
http://dx.doi.org/10.1016/j.jmps.2013.08.007

modulus on the order of 1 GPa (Allain et al., 2008; Bouaziz, 2012; Bouaziz et al., 2010, 2008; Bouaziz and Guelton, 2001; Chen et al., 2007; Ding et al., 2011; Idrissi et al., 2010b; Jin and Lee, 2009; Liang et al., 2009; Sevillano, 2009; Shiekhelsouk et al., 2009). Due to the high strain hardening, TWIP steels can attain an elongation about 60–95%, and the corresponding ultimate strength is about 800 MPa to 1.8 GPa (Allain, 2002; Allain et al., 2002; Bayraktar et al., 2004; Chen et al., 2007; Dastur and Leslie, 1981; Frommeyer et al., 2003; Grässel et al., 2000; Huang et al., 2006; Kim et al., 2009; Lai and Wan, 1989; Mi et al., 2005, 2012; Vercammen, 2004). The diagram given in Fig. 1 summarizes the mechanics properties of several steels and other metallic materials of current interest, among which TWIP steels owe the most promising combination of strength and deformability.

The attractive properties in TWIP steels are attributed to the activation of twinning during their plastic deformation. At room temperature, deformation twinning is not regarded as the primary plastic carrier in conventional face centered cubic (FCC) metals because their stacking fault energy (SFE) is relatively high. It is reported that low intrinsic stacking fault energy γ_{sf} (below approximately 20 mJ/m^2) favors the γ (FCC phase) to ε (hexagonal close-packed, HCP phase) transformation in TWIP steels; while $\gamma_{sf} > 20$ mJ/m^2, this phase transformation is rarely observed (Sato et al., 1989). When γ_{sf} is too high, motion of complete dislocations takes over and becomes the primary plastic deformation mechanism. Such a transition can be readily explained if the nucleation of $a/6\langle 112\rangle$ Shockley partial dislocations and $a/2\langle 110\rangle$ complete dislocations are the controlling factors for the competition between deformation twinning and dislocation glide. The critical resolved shear stress (CRSS) τ_{crss} for the nucleation of an $a/6\langle 112\rangle$ Shockley partial dislocation is about $\tau_{crss}=\gamma_{sf}/b+\alpha Gb/3d$ (Asaro et al., 2003; Asaro and Suresh, 2005; Wei et al., 2006; Zhu et al., 2005), while the CRSS τ_{crss} for the nucleation of a complete dislocation approximates to $\beta Gb/d$, where b is the Burgers vector, G is the shear modulus, d is the grain size, and α and β are coefficients on the order of unit. The expressions for τ_{crss} indicate that materials with higher SFE tend to nucleate complete dislocations. That is to say, the SFE of FCC austenite needs to be in the right range, neither too low nor two high, in order to promote deformation twinning while the material is deforming at a certain range of temperatures and strain rates. Current understanding on the roles of manganese and carbon (or its alternatives) in TWIP steel enables us to tune the composition of the materials and achieve the suitable SFE to promote deformation twinning (Allain et al., 2010; Brüx et al., 2002; Curtze and Kuokkala, 2010; Curtze et al., 2011; Dumay et al., 2008; Idrissi et al., 2010a, 2009; Jeong et al., 2012; Jin and Lee, 2012; Lee et al., 2010; Park et al., 2010; Saeed-Akbari et al., 2011; Wang et al., 2010; Yoo and Park, 2008). It is worth pointing out that appropriate SFE is necessary but by no means a sufficient condition for twinning (Bouaziz et al., 2011a; Meyers et al., 2001). As commented by Christian and Mahajan (1995), loading modes, temperature, residual strain, grain size, and strain-rate all influence the activation of deformation twinning.

From the crystallographic aspect, motion of a complete dislocation gives rise to shear displacement of a portion of the crystal over another and leaves the lattice virtually unchanged. In contrast, shear displacement induced by a Shockley partial dislocation is only a fraction of the inter-atomic spacing. During twinning, the nucleation and gliding of several leading partials in successive planes result in mirror image lattice reorientations across the boundary. Now in addition to the initial crystallographic texture characteristics of TWIP steels resulted from rolling processing, deformation twinning further alters the texture dramatically. The reorientation induced by twinning brings exceptional yet unique characteristics in crystalline materials. For example, it is evident that the consequently formed mirror planes are effective barriers to dislocation slips inclined to those planes (Li et al., 2010). It hence enhances the strength of the material as deformation proceeds. As a result,

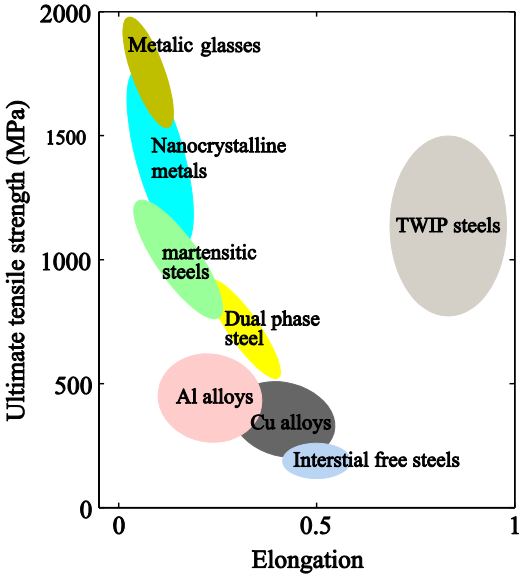

Fig. 1. Illustration to show the ultimate tensile strength versus elongation for several conventional metals, as well as metallic glasses and nanocrystalline metals. TWIP steels owe both high strength and large tensile elongation.

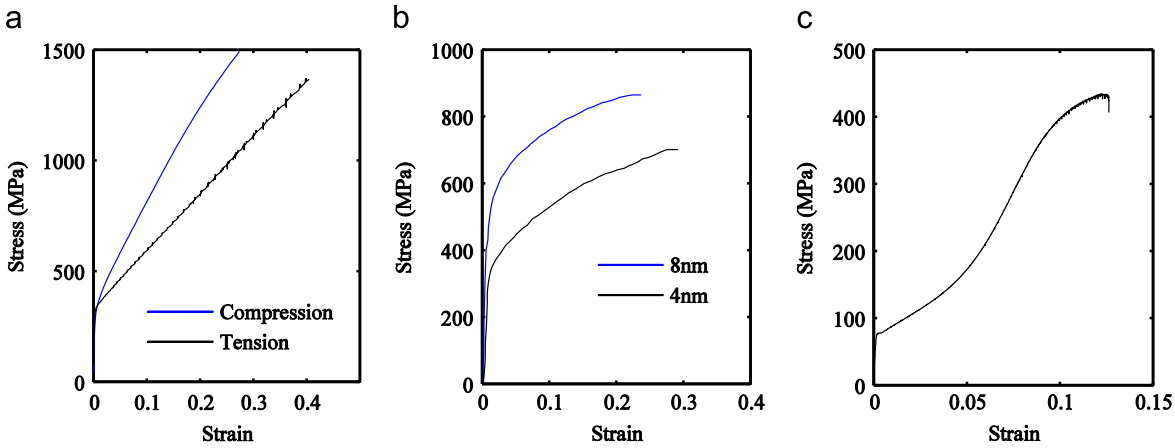

Fig. 2. Strain hardening in crystalline metals where twinning plays a significant role in plastic deformation. (a) Compressive and tensile stress–strain curves for a high-manganese steel (Fe23.84Mn0.61C, wt%); (b) the stress–strain curves (replotted) for nano-twinned crystalline Cu samples with average twin thicknesses of 4 nm and 8 nm (Lu et al., 2009). Deformation twinning is regarded as one of the primary plastic deformation mechanisms in such samples with preexisting twins; (c) Compressive stress–strain curve for magnesium alloy AZ31B.

Table 1
Chemical compositions (in weight percentage, wt%) of the FeMnC TWIP steel investigated in this study.

Name	Fe	Mn	C
Fe23.84Mn0.61C	0.7554	0.2384	0.0061

those materials where deformation twinning plays a significant role in plasticity commonly exhibit high strain hardening. Fig. 2 presents several typical examples of crystalline metals where deformation twinning plays a crucial role for their plastic deformation.

In order to understand the mechanisms accounting for the enormous strain hardening in TWIP steels, there is a pressing need to reveal the correlation between texture evolution and strain hardening by deformation twinning. In addition, while it is generally accepted that mechanical twinning is competitive to dislocation motion in TWIP steels, the role played by each mechanism at different stages of deformation is hard to abstract from experiments, due to the factor that current experimental observations are usually carried out on post-mortem samples. Last but not least, the remarkable deformability in TWIP steels is desired in industrial plastic forming (Chung et al., 2011; Cooman et al., 2011, 2005; Scott et al., 2006), and it is now important to supply reliable simulating tools for the manufacturing processing for TWIP steels, while using the materials to make complex parts by stamping. With the motivations given above, here we conduct both experimental characterizations and numerical simulations, in hope to reveal the hardening mechanisms and the texture evolution in TWIP steels during plastic deformation.

2. Experimental results

Since the pioneering work of Hadfield (Adler et al., 1986; Dastur and Leslie, 1981; Karaman et al., 2000; Raghavan et al., 1969), steels with fully austenitic microstructures but different compositions have been made. Two categories of the family, which were named by their characteristics in plastic deformation, TRIP and TWIP steels, have been intensively investigated in the last decade. It is generally accepted that TWIP steels have high manganese content in the range of 12–30 wt%. Here we choose one TWIP steels with elements of Fe, Mn, and C for our investigation. For simplicity, we use FeMnC as the name of the TWIP steel in what follows. In Table 1, we show the specific chemical compositions for the FeMnC TWIP steel in the present study.

The elements were melted in vacuum induction furnace and protected with Ar gas. We then cast the molten steel to flat ingot. Rolling is conducted at the initial rolling temperature of 1050 °C, and at the finishing temperature of 975 °C. The final hot rolling plate is about 26.0 mm thick. The plates are then gone through air cooling. After cooling, we cut specimens from those plates for further mechanical tests. For convenience, we use the coordinate system defined by the rolling direction (RD), the transverse direction (TD), and the normal direction (ND) to characterize the tested samples. Fig. 3a shows the tensile stress–strain behavior for the TWIP steel at low strain rates. True stress–strain responses in the RD, TD and ND show slight difference, which is consistence with the previous observation that there is weak initial texture (Bouaziz et al., 2011a). Corresponding compressive stress–strain responses in the three directions are given in Fig. 3b.

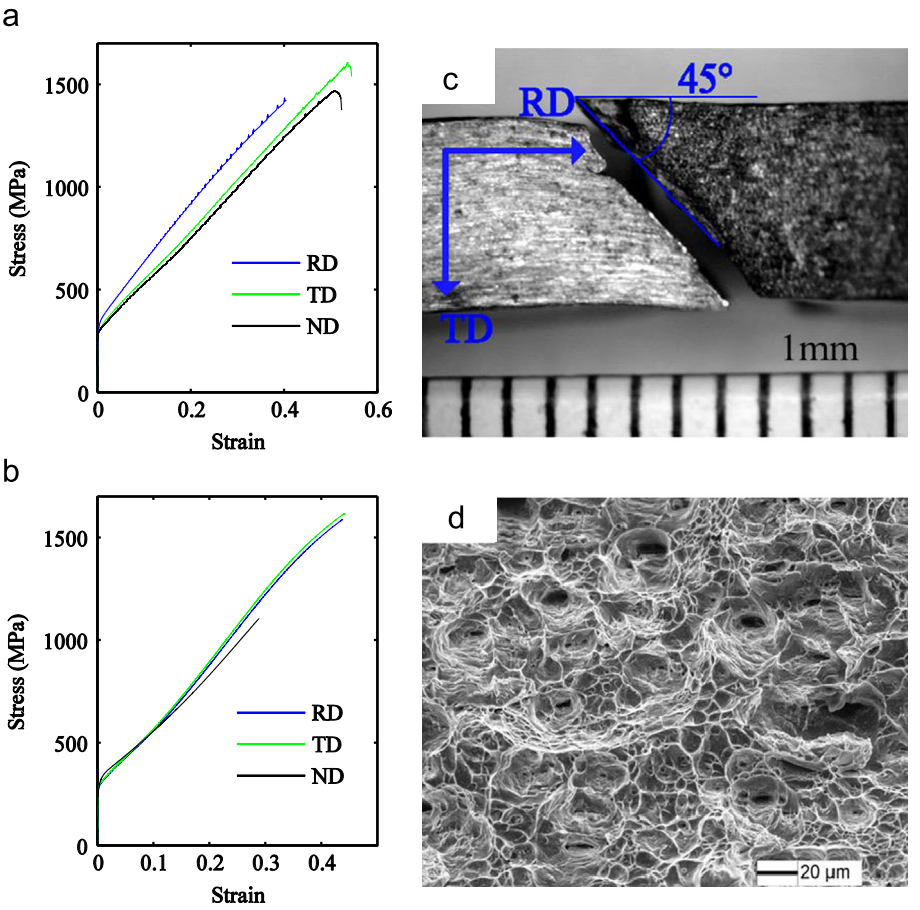

Fig. 3. The quasi-static stress–strain response of FeMnC. (a) Tensile stress–strain curves in the rolling direction (RD), the transverse direction (TD), and the normal direction (ND). (b) Compressive stress–strain curves in the three directions. (c) Macroscopic fracture patterns for TWIP steels with tensile loading in the RD direction. (d) Fractographic examination to show the ductile feature of the fracture surfaces in TWIP steels, where large amount of bird nest type dimples are seen.

Due to the extraordinary deformability for TWIP steels, none of the samples subjected to compression were fractured after the applied deformation. The macroscopic failure pattern of the tensile samples in the RD is given in Fig. 3c. The fracture results from typical shear failure, with the shear angle between the failure plane and the loading axis about 45°. Large amount of bird nest type dimples left by severe plastic flow are seen in the fractographic observation, as evidently observed in the scanning electron microscope (SEM) pictures shown in Fig. 3d. In addition to the fractographic observation presented in Fig. 3, we show in Fig. 4 the characteristic of microscopic structures after different deformation modes. As a comparison, the initial microstructure of the FeMnC TWIP steel is given in Fig. 4a. There is perceivable amount of preexisting annealing twins in the material. After quasi-static tension, enormous amount of lenticular twins and slip lines in austenitic grains are formed, see Fig. 4b. The same type of deformation twinning is seen in samples after quasi-static compression, as shown in Fig. 4c. Inspired by the large amount of twinning and dislocation activities, we will try to quantify the activated deformation twinning and dislocation slips by measuring the orientation density of the materials before and after deformation.

We show in Fig. 5a the initial texture in FeMnC in the rolling direction. For here and in what follows, all pole figures are equal-area projections of the specified crystallographic planes. The main components of texture in TWIP steels are cubic-type texture {001} ⟨100⟩, rotated brass-type texture {110} ⟨111⟩ and the E-type texture {111} ⟨110⟩ (Lü et al., 2010; Vercammen et al., 2004). The intensity of texture in the TWIP steel, however, is rather weak. This observation is consistent with existing experiments (Bracke et al., 2009; Lü et al., 2011; Saleh et al., 2011). After tension, the primary orientations of the TWIP steel become the cubic-type texture {001} ⟨100⟩ and the rotated brass-type texture {110} ⟨111⟩ (see Fig. 5b). Given grains from ⟨111⟩ orientation are adequate for twinning whereas ⟨100⟩ fiber orientation are more suitable for slip, the final texture reflects a combination impact of twinning and slip (Barbier et al., 2012, 2009a, 2009b; Gutierrez-Urrutia et al., 2010; Meng et al., 2007; Yang et al., 2006). In contrast, after quasi-static compression, the main components of textures are the rotation Goss-type texture {110} ⟨110⟩, Goss/Brass type texture (in between the Goss type texture and the brass-type texture), as well as Goss twin-type texture {113} ⟨332⟩ (see Fig. 5c).

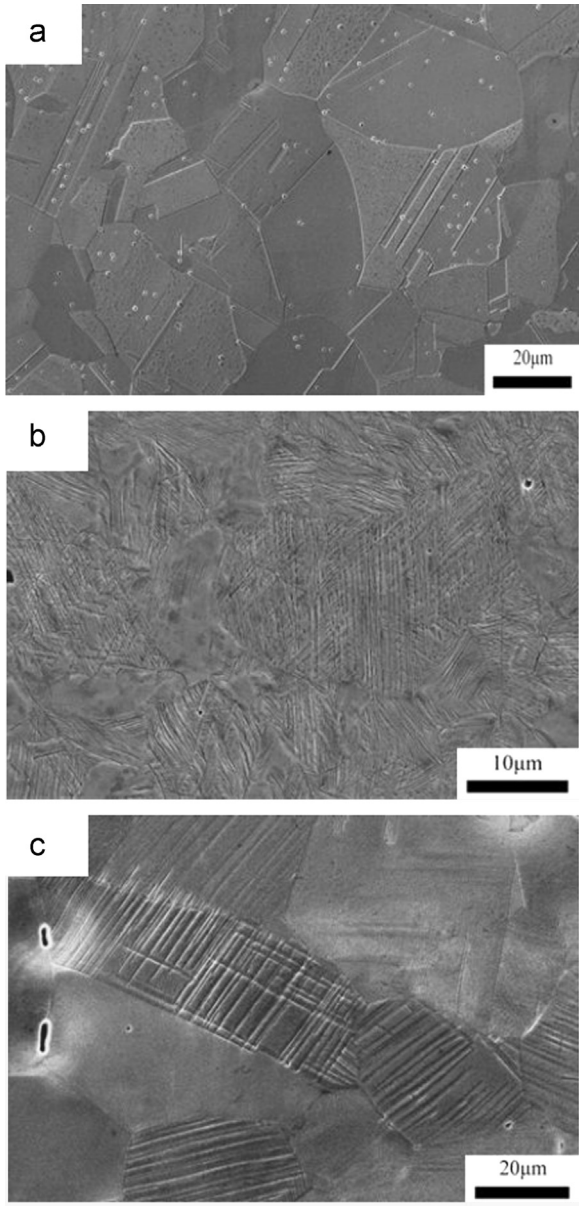

Fig. 4. Scanning electron microscopy of TWIP steels to show microstructures at different stages of deformation. (a) Initial sample with average grain size about 35 μm. (b) Microstructures after quasi-static tension (strain rate: $10^{-3}\,s^{-1}$, tensile strain about 56%). (c) Deformation pattern after quasi-static compression (strain rate: $10^{-3}\,s^{-1}$, compressive strain about 43%).

3. A mechanistic model for strain hardening by twin thickening

As seen from the microstructures in the deformed samples, there exists large amount of deformation twinning in the TWIP steel after deformation. Now we aim to develop a simple model to capture the strain hardening seen in the stress–strain curves in Fig. 3. By assuming that plasticity is dominated by deformation twinning, we see several scenarios which could result in strengthening in TWIP steels. (a) Dislocation pileup by deformation twinning: from the perspective based on the interaction between dislocations and grain boundaries, a deformation twin usually results in the formation of two dislocation walls at the two ends of a twinned lentil. If those dislocations are not absorbed by the GBs, they will contribute to strengthening. (b) Twin boundary as barriers to dislocations or secondary twins: it is well known that by increasing grain boundaries (GBs) numbers as grain sizes reduce; we could achieve substantial increasing in strength in crystalline metals (Li et al., 2010; Lu et al., 2009, 2004). The formation of low energy and coherent twin boundaries (TBs) supplies a desired strengthening mechanism in polycrystalline metals (Allain et al., 2004a, 2004b, 2004c; Bouaziz and Guelton, 2001; Brüx et al., 2002). (c) Depletion of easy twinning regions: if twinning is the only plastic deformation in a polycrystalline metal, the gradual depletion of easy-to-be-twinned grains while straining hardens the materials as well.

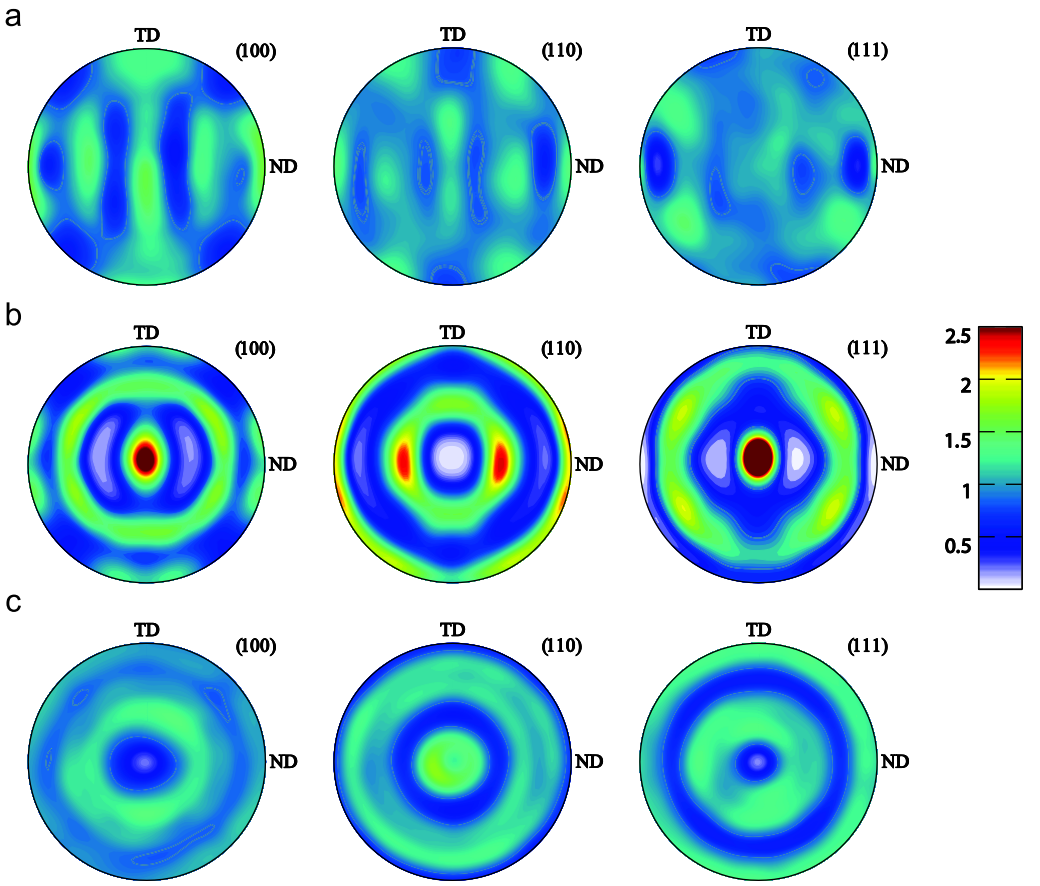

Fig. 5. Texture of FeMnC TWIP steel in RD at different status. (a) Initial texture in three different crystallographic planes. (b) Texture after 56% tensile strain. (c) Texture after 43% compression strain.

Here we present a tentative theoretical analysis regarding how deformation twinning can give rise to nearly constant strain hardening modulus. We start with using the free energy F associated with the nucleation of a twin laminar with width λ in a grain with size d (Wei, 2011a):

$$F=\left[\frac{\pi}{8}\frac{2-\nu}{1-\nu}\frac{\lambda}{d}G(e^T)^2-(\tau-\tau_l)e^T\right]V+2\gamma_{sf}S, \tag{1}$$

where G is the shear modulus, ν is Poisson's ratio, $V=\pi d^2\lambda/4$ and $S=\pi d^2/4$, e^T is the shear strain associated with twinning/de-twinning, γ_{sf} is the twin-boundary energy, and τ and τ_l are the applied shear stress and the lattice resistance, respectively. This energy term is derived by treating the twin laminar as an inclusion with uniform shearing (Eshelby, 1957). By applying the above equation to dislocation-mediated twinning in an incremental manner, we obtain the free energy associated with the thinnest twins as

$$\frac{F}{V}=\frac{\pi}{8}\frac{2-\nu}{1-\nu}\frac{3d_{(111)}}{d}G(e^T)^2-(\tau-\tau_l)e^T+\frac{2\gamma_{sf}}{3d_{(111)}}. \tag{2}$$

here $d_{(111)}$ is the space of between two neighboring (111) planes. It requires at least three layers of (111) atomic planes to define a twin fault (Mahajan and Chin, 1973). With $F\leq 0$ for successful nucleation of a twin embryo, we obtain the corresponding critical stress to be

$$\tau=\tau_l+\frac{\pi}{8}\frac{2-\nu}{1-\nu}\frac{3d_{(111)}}{d}Ge^T+\frac{2\gamma_{sf}}{3e^Td_{(111)}}. \tag{3}$$

Assuming that the dislocations are not being absorbed by grain boundaries, after the twinning of n successive layers, the free energy change to add another atomic plane to the twinned region would be

$$\Delta F=F(n+1)-F(v)=\left[\frac{\pi}{8}\frac{2-\nu}{1-\nu}\frac{(2n+1)d_{(111)}}{d}G(e^T)^2-(\tau-\tau_l)e^T\right]\frac{\pi d^2}{4}d_{(111)}. \tag{4}$$

Table 2
Material parameters for nanotwinned Cu (ntwin-Cu) and FeMnC. When deformation twinning is the dominant mechanism for plasticity, the predicted hardening modulus H using Eq. (7) is close to the experimental measurement H_{exp}.

	G (GPa)	ν	γ_{sf} (mJ/m^2)	e^T	$d_{(111)}$ (nm)	b (nm)	λ (nm)	d (μm)	H (GPa)	H_{exp} (GPa)
ntwin-Cu	40	0.34	45	0.707	0.156	0.148	~5	0.5	1.8	1.5–2.5
FeMnC	65	0.3	20	0.707	0.208	0.197	~100	10	2.7	2–5

By applying $\Delta F \le 0$, we yield the critical stress for the initiation of dislocation motion for the $(n+1)$-th layer to be

$$\tau_{flow} = \frac{\pi}{4}\frac{2-\nu}{1-\nu}\frac{(n+1)d_{(111)}}{d}Ge^T + \tau_l + \frac{\pi}{8}\frac{2-\nu}{1-\nu}\frac{d_{(111)}}{d}Ge^T. \tag{5}$$

Therefore, if we assume the dislocations are not absorbed by the GB, the flow stress would steadily increase with each additional layer of twinning. The hardening by the growth of twins can be obtained based on Eq. (5) by assuming that deformation twinning is the only plastic carrier. For a twinned region with thickness λ, further thickening by emission of one partial dislocation gives a plastic strain increment $\varepsilon_0 = b/\lambda$ (Wei, 2011a). With Eq. (5), the hardening by twin growth is

$$\frac{d\tau_{flow}}{d\varepsilon} \approx \frac{\tau_{flow}(n+1)-\tau_{flow}(n)}{\varepsilon_0} = \frac{\pi}{4}\frac{2-\nu}{1-\nu}\frac{d_{(111)}}{d}Ge^T\frac{1}{\varepsilon_0}. \tag{6}$$

By taking into account the influence of crystallographic orientations, the hardening modulus by twin growth can be rewritten as

$$H = \beta_T\frac{d\tau_{flow}}{d\varepsilon} = \beta_T\frac{\pi}{4}\frac{2-\nu}{1-\nu}\frac{d_{(111)}}{b}\frac{\lambda}{d}Ge^T. \tag{7}$$

where $\beta_T=3$ is the Taylor factor. We show in Table 2 the hardening modulii predicted by the theoretical analysis for two typical materials where deformation twinning is regarded as their primary carrier for plasticity. The theoretical results for the two materials match reasonably well with experimental measurements. Eq. (7) also implies that twinning dominated plasticity may give rise to higher strain hardening modulus as twins are thickening (λ increases) as plasticity accumulates, which is in qualitative agreement with experiment observations for metals where deformation twinning is their primary deformation mechanism for plasticity (see Fig. 2c and Fig. 3a and b).

4. Crystal plasticity model for twinning and dislocation slip

In addition to the theoretical analysis, we are interested in exploring the deformation in TWIP steel by physically rooted constitutive models. We employ the classical framework of rate-independent single-crystal plasticity (Asaro and Needleman, 1985; Dancette et al., 2012; Kalidindi et al., 1992; Roters et al., 2010) to model plasticity by dislocation slip. There also exists pioneering work to model deformation twinning in the continuum mechanics frame (Kochmann and Le, 2009; Staroselsky and Anand, 1998; Staroselsky, 1998). Staroselsky and Anand put forward a crystal plasticity model for FCC materials by taking both slip and twinning accommodated plasticity into account (Staroselsky and Anand, 1998); Fernández et al. improved the model by considering cross-hardening between slip and twinning systems (Fernández et al., 2011). The influence of pre-existing twins to the ductility and strength behavior of materials has also been investigated by Jérusalem et al. (2008) using finite-element based crystal plasticity simulations; Proust et al. implemented a meso-scale composite grain model to understand the texture, twinning and hardening evolution of pure Zr (Proust et al., 2007). Here we adopt the single crystal scheme developed by Starowsky and Anand (Staroselsky and Anand, 1998; Staroselsky, 1998). For completeness, we repeat here part of the key ingredients. In such framework, the deformation gradient $\boldsymbol{F}$ is decomposed into elastic ($\boldsymbol{F^e}$) and plastic ($\boldsymbol{F^p}$) parts as

$$\boldsymbol{F} = \boldsymbol{F}^e\boldsymbol{F}^p, \tag{8}$$

with $\det(\boldsymbol{F}^e) > 0$ and $\det(\boldsymbol{F}^p)=1$. Plastic flow takes place through both dislocation slip and deformation twinning in prescribed crystallographic slip/twinning systems. Here, we use integer i to label crystal slip systems and integer α to label crystal twin systems. At the initial configuration, each slip system is defined by a slip/twinning direction $\boldsymbol{m}_0$ and a slip/twinning-plane normal $\boldsymbol{n}_0$. The Green elastic strain measure $\boldsymbol{E}^e$ and the symmetric second Piola–Kirchhoff stress tensor $\boldsymbol{T}$ are hence defined respectively as

$$\boldsymbol{E}^e \equiv (1/2)(\boldsymbol{F}^{eT}\boldsymbol{F}^e - 1) \text{ and } \boldsymbol{T} \equiv \boldsymbol{C}\boldsymbol{E}^e, \tag{9}$$

where the superscript 'T' stands for the transpose of a tensor and $\boldsymbol{C}$ is the fourth order tensor of elastic moduli. The resolved shear stress τ on the slip/twinning system $(\boldsymbol{m}_0, \boldsymbol{n}_0)$ is calculated as

$$\tau = (\boldsymbol{F}^{eT}\boldsymbol{F}^e\boldsymbol{T}) \cdot (\boldsymbol{m}_0 \otimes \boldsymbol{n}_0). \tag{10}$$

The evolution of plastic deformation gradient, on multiple i/α-th slip/twin systems, is given as

$$\boldsymbol{F}^p = 1 + \sum_i \Delta\gamma^i \boldsymbol{S}_0^i + \sum_\alpha \Delta\gamma^\alpha \boldsymbol{S}_0^\alpha, \boldsymbol{S}_0^i \equiv \boldsymbol{m}_0^i \otimes \boldsymbol{n}_0^i \text{ and } \boldsymbol{S}_0^\alpha \equiv \boldsymbol{m}_0^\alpha \otimes \boldsymbol{n}_0^\alpha \tag{11}$$

where $\boldsymbol{S}_0^i$ is the Schmid tensor for the i-th slip system, and $\boldsymbol{S}_0^\alpha$ is the Schmid tensor for the α-th twin system. $\Delta\gamma$ is the incremental shear due to slip/twinning, which is determined by using the consistency condition in rate-independent plasticity scheme given the resolved shear stress τ and the resistance S on the slip/twinning system.

One of the major uncertainties is how to capture the slip/twin hardening. Simple phenomenological models for the evolution of $S^i$and S^α are formulated below. The slip system deformation resistances are taken to evolve in the form (Kalidindi et al., 1992):

$$S^i(\tau) = S^i(t) + \sum_j h_{sl}^{ij}(t)\Delta\gamma_{sl}^j, \quad \text{where } h_{sl}^{ij} = q_{sl}^{ij} h_{sl}^j. \tag{12}$$

here h_{sl}^{ij} are components of the hardening matrix,

$$q_{sl}^{ij} = [q_{sl} + (1 - q_{sl})\delta^{ij}] \tag{13}$$

is the matrix describing the latent hardening, with $q_{sl} = 1.0$ for co-planar systems and $q_{sl} = 1.4$ for non-coplanar systems, and

$$h_{sl}^j = h_{sl,0}\left(1 - \frac{S_{sl}^j}{S_{sl}}\right)^{a_{sl}} \tag{14}$$

is the single slip hardening rate. So we have $\{h_{sl,0}, S_{sl}, a_{sl}\}$ as hardening parameters for dislocation slip, which are taken to be identical for all slip systems. The twin system deformation resistances are taken to evolve in the form

$$S^\alpha(\tau) = S^\alpha(t) + \sum_j h_{tw}^{\alpha j}(t)\Delta\gamma_{tw}^j, \quad \text{where } h_{tw}^{\alpha j} = q_{tw}^{\alpha j} h_{tw}^j. \tag{15}$$

Similarly, h_{tw}^{ij} are the components of the hardening matrix by deformation twinning, and

$$q_{tw}^{\alpha j} = [q_{tw} + (1 - q_{tw})\delta^{\alpha j}] \tag{16}$$

is the latent hardening matrix, with $q_{tw} = 1.0$ for co-planar systems and $q_{tw} = 1.4$ for non-coplanar systems. For the single twinning hardening rate,

$$h_{tw}^j = h_{tw,0}\left(1 - \frac{S_{tw}^j}{S_{tw}}\right)^{a_{tw}}. \tag{17}$$

The three $\{h_{tw,0}, S_{tw}, a_{tw}\}$ hardening parameters are taken to be identical for all twinning systems.

Twinning is considered as pseudo-slip. Different to dislocation slip, however, deformation twinning will result in the rotation of the lattice in the region of the crystal that has gone through twinning (Kelly and Knowles, 2012; Pitteri, 1985, 1986). For TWIP steels, we consider the twin elements $\{\boldsymbol{K}_1, \boldsymbol{K}_2, \boldsymbol{\eta}_1, \boldsymbol{\eta}_2\}$ defined by

$$\boldsymbol{K}_1 = (111), \quad \boldsymbol{\eta}_1 = [11\bar{2}], \quad \boldsymbol{K}_2 = (11\bar{1}), \quad \boldsymbol{\eta}_2 = [112]. \tag{18}$$

With the definition of $\boldsymbol{p}$ being a unit vector in the $\boldsymbol{\eta}_1 = [11\bar{2}]$ direction, and $\boldsymbol{q}$ being the unit normal to the $\boldsymbol{K}_1 = (111)$ plane. The rotations which carry the matrix lattice to twinned lattice and the inverse (or detwinning) are respectively given by,

$$\boldsymbol{R}^{tw} = 2\boldsymbol{q} \otimes \boldsymbol{q} - 1 \quad \text{and} \quad \boldsymbol{R}^{dw} = 2\boldsymbol{p} \otimes \boldsymbol{p} - 1. \tag{19}$$

That is, if $\boldsymbol{x}_a$ are the lattice vectors of the matrix crystal, then the lattice vectors in the twinned region are given by $\boldsymbol{e}_a = \boldsymbol{R}^{tw}\boldsymbol{x}_a$. As soon as the accumulative pseudo-slip in a twinning system reaches the threshold strain $0.5e^T$, we will rotate the matrix lattice to the twinned lattice in each single crystal. Further details can be found in Staroselsky and Anand (1998), Staroselsky (1998).

5. Numerical modeling on deformation mechanisms in TWIP steels

Now we use the constitutive model summarized above to simulate the mechanical deformation of TWIP steels with large plasticity. Material parameters are abstracted by fitting the experiments results in RD. We then explore the roles by each mechanism at different stages of plastic deformation, and test the predictability of the model to deformation in ND. Given the large deformability of the materials and the grain sizes are in tens of micrometers, we neglect the influence of grain boundary deformation, as the latter usually results in premature failure and low ductility. That means that grains in our samples are rigidly bonded. Detailed material parameters include

- Elastic properties: the used values of elastic constants for FeMnC are $C_{11} = 235.5$ GPa, $C_{12} = 138.0$ GPa, $C_{44} = 117.0$ GPa (Gebhardt et al., 2011; Idrissi et al., 2010a).
- Slip/twinning systems: the 12 slip systems in FCC crystals are $\{111\}\langle 110\rangle$, the 12 twin systems in FCC crystal are $\{111\}\langle 11\bar{2}\rangle$.

- Initial slip/twinning resistances: {121 MPa} for slip and {70 MPa} for twin. These numbers reflect the factor that the nucleation of leading partial dislocations for twins is much easier than the generation of complete dislocations. These numbers are calibrated to ensure experimentally measured stress–strain curves and texture at a given strain match well with simulated results when deformation is applied along the RD direction.
- Initial texture: the experimentally measured orientation data (Fig. 5) for the as received FeMnC are discretized into 300 orientations for the 300 Voronoi grains.
- Hardening parameters for slip and twinning: in the power-law hardening, we have three parameters $\{h_{sl,0}, S_{sl}, a_{sl}\}$ for slip induced hardening, and three parameters $\{h_{tw,0}, S_{tw}, a_{tw}\}$ for twin induced hardening. Motivated by the mechanistic

Table 3
Two sets of strain hardening parameters used in the crystal plasticity model for our finite-element simulation.

	S_0^i (MPa)	$h_{sl,0}$ (MPa)	S_{sl} (GPa)	a_{sl}	S_0^α (MPa)	$h_{tw,0}$ (MPa)	S_{tw} (GPa)	a_{tw}
Twin only	–	–	–	–	90	280	1	1.0
Twin & slip	121	400	2	0.25	70	2000	1.2	1.0

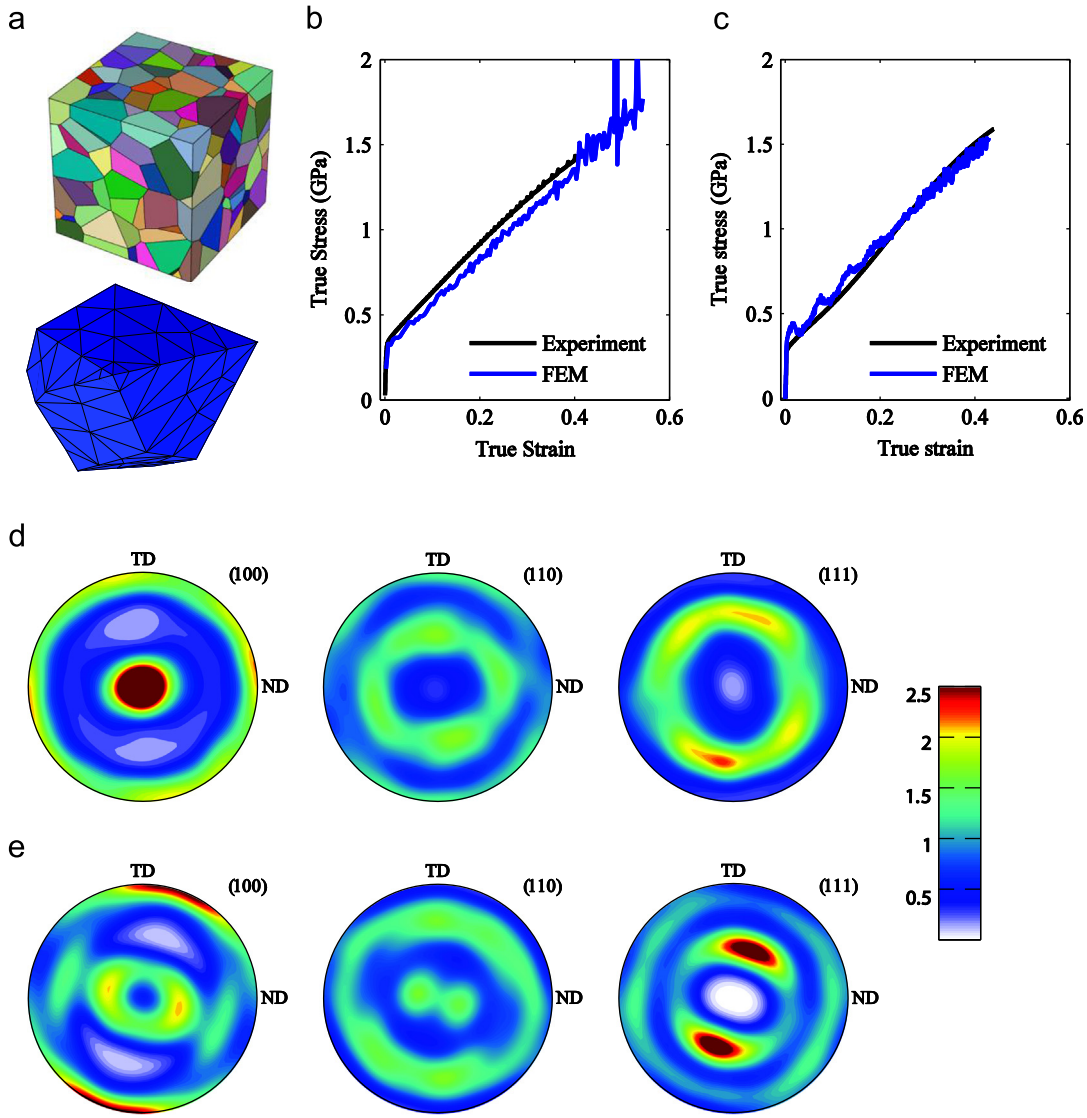

Fig. 6. Experimental results versus simulated results for FeMnC TWIP steel while straining in RD direction. Here we only consider plasticity by deformation twinning. (a) Initial microstructures and typical mesh in a grain. Stress–strain curves for (b) tension and (c) for compression. Crystallographic texture for FeMnC from simulations. (d) Texture after 56% tensile strain. (e) Texture after 43% compressive strain.

model for strain hardening by deformation twinning (Eq. 7), we have used a linear hardening law for deformation twinning, i.e. $a_{tw} = 1$ in Eq. (17).

To get a clear picture about the role played by each mechanism for hardening, we do not take the cross-hardening into account in the present study. The readers are referred to a more sophisticated treatment for cross-hardening in crystal plasticity models considering both twinning and dislocation slip (Fernández et al., 2011). We have used two sets of material parameters to capture the strain hardening in TWIP steel FeMnC: in one case, we suppress dislocation induced plasticity and see whether deformation twinning alone can capture the stress–strain behavior and the texture evolution of the material. Both dislocation slip and deformation twinning are activated in the second case. Corresponding hardening parameters for both cases are listed in Table 3.

In Fig. 6a, we show the polycrystalline microstructure used for all simulations. The mesh of a typical grain is also given at the bottom in Fig. 6a. We first explore the stress–strain behavior by taking into account plasticity by deformation twinning alone. A reasonable match between the stress–strain curves from experiments and those from modeling is observed. Fig. 6b

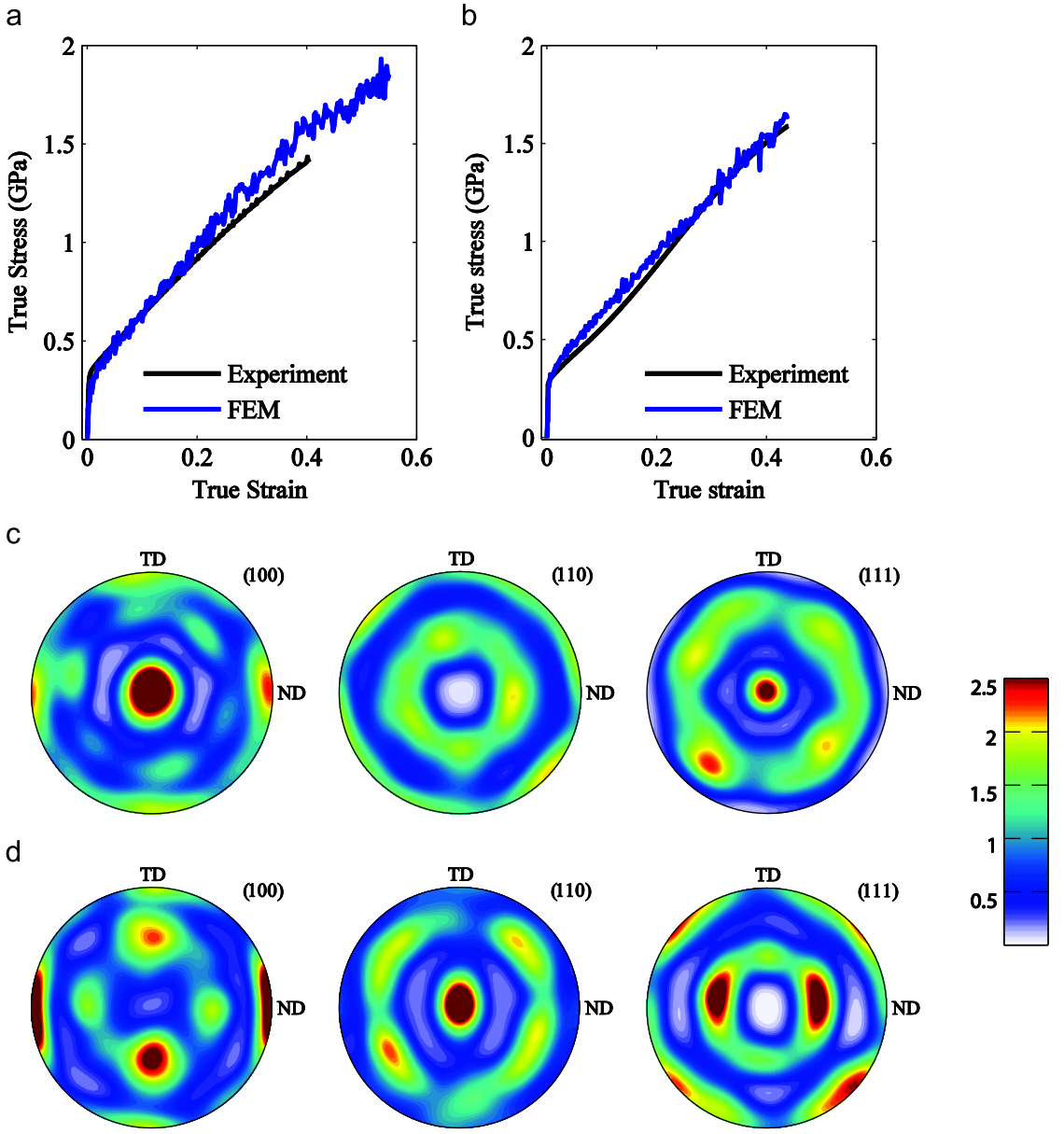

Fig. 7. Experiments versus simulated results by considering both dislocation slip and deformation twinning in RD direction. Stress–strain behavior: (a) tensile stress–strain curves, and (b) compressive stress–strain curves. Texture evolution: (c) texture at 56% tensile strain, simulation, and (d) texture at 43% compressive strain, simulation.

presents the stress–strain curves in tension, and the compressive stress–strain curves are given in Fig. 6c. As plastic deformation increases, the 12 twin resistances increase correspondingly from 90 MPa to about 548 ± 96 MPa at a true strain of 0.56 in tensile tests, and it increases to 460 ± 62 MPa at a true strain of -0.43 in compressive. By further checking the

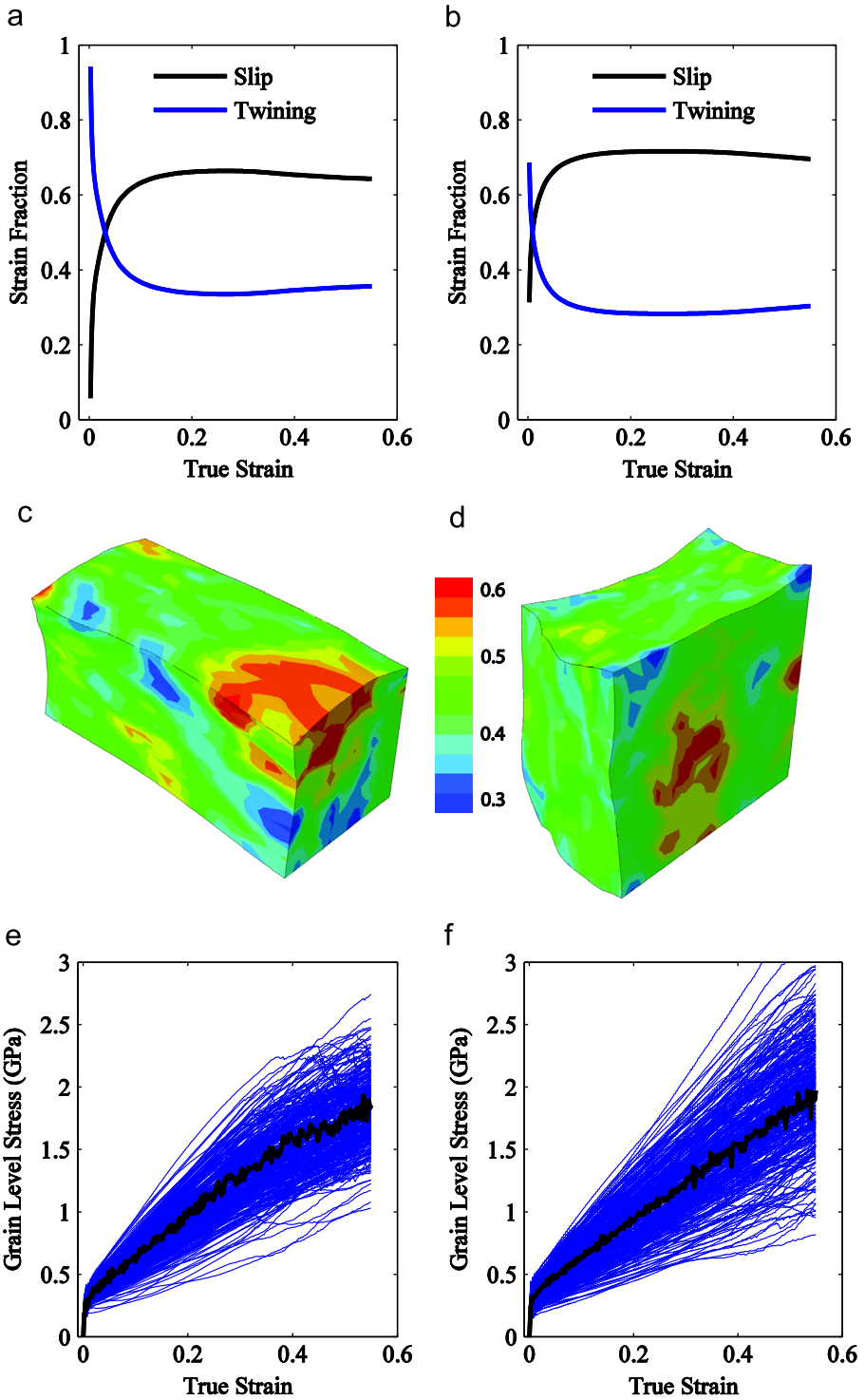

Fig. 8. Detailed grain level deformation from simulations while loading along the RD direction. (a) The fractional plastic strain contributed by individual mechanisms during tension. (b) Evolution of fractional plastic strain during compression. Contours of equivalent plastic strain at (c) 56% tensile strain, and (d) at 43% compressive strain. Grain level stress as a function of strain during (e) tension and (f) compression. Blue lines are for average stresses along the loading axis for individual grains, and the black line is the macroscopic stress–strain response of the sample. (For interpretation of the references to color in this figure legend, the reader is referred to the web version of this article.)

crystallographic textures for FeMnC after deformation, the results from our simulations (Fig. 6d for tension and 6e for compression) differ from the experimental measurements in Fig. 5: The strong {111} texture fiber is missing. The inconsistency in texture evolution implies that deformation twinning may be not the single carrier for plasticity.

By activating both dislocation slip and deformation twinning in the constitutive model, we show in Fig. 7 the simulated stress–strain curves again experimental results, with Fig. 7a for tension and Fig. 7b for compression. A nice match in stress–strain curves between our simulations and the experimental results is obtained by using the material parameters given in Table 3. Interestingly, stress–strain curves from our simulations also capture the increasing strain hardening modulus with straining, which is regarded as a crucial factor for the large ductility in TWIP steels. The {100}, {110}, and {111} pole figures for quasi-static tension and for quasi-static compression are shown in Fig. 7c and d; the {100}, {110} and {111} pole figures are very much alike between the numerical prediction and experimental measurements (Fig. 5b for tension and 5c for compression). To see the competition between the dislocation mechanism and the twinning deformation, we define two equivalent plastic strains, with

$$\Delta\bar{\gamma}_{sl}=\sqrt{(3/2)(\sum_i \Delta\gamma^i_{sl}S^i_0):(\sum_i \Delta\gamma^i_{sl}S^i_0)},\quad \Delta\gamma_{sl}=\int_0^\tau \Delta\bar{\gamma}_{sl}\,dt \tag{20a}$$

and

$$\Delta\bar{\gamma}_{tw}=\sqrt{(3/2)(\sum_\alpha \Delta\gamma^\alpha_{tw}S^\alpha_0):(\sum_\alpha \Delta\gamma^\alpha_{tw}S^\alpha_0)},\quad \Delta\gamma_{tw}=\int_0^\tau \Delta\bar{\gamma}_{tw}\,dt \tag{20b}$$

contributed by dislocation slip and deformation twinning, respectively. The evolution of fractional equivalent plastic strains as a function of the applied strain is shown in Fig. 8a for tension and 8b for compression. During the incipient of plastic deformation, we find that twinning dominates the plastic deformation and its fractional plastic strain reaches about 90% within 5% strain. The fractional strain by twinning drops quickly with straining while that by dislocation slip increases. Beyond 20% strain, both fractional strains reach their steady state: dislocation slip occupies about 65% of the overall plastic strain, and deformation twinning takes about 35%. That is to say, even the materials are named as 'twinning induced plasticity steel', more plastic deformation comes from dislocation slip, that circumstance only happens at the initial stage of plasticity. In Fig. 8c and d, we show the equivalent plastic strain contour at 56% tensile strain and 43% compressive strain, respectively. While there is no apparent shear localization at the grain level, severe inhomogeneity in plastic deformation is observed. The average stress at typical grains are shown in Fig. 8e (in tension) and 8f (in compression). Strong fluctuation for stress at the grain level is also seen, and the fluctuation becomes large at higher level stress.

So far, our simulations have shown the capability of the crystal plasticity model to capture the essence of deformation characteristics in TWIP steel with severe plastic deformation. Now we aim to testify its predictability. We consider the same material but investigate its deformation in the ND direction. To be consistent, we use the same material parameters for previous simulations for the deformation in the RD direction. The initial texture for the sample in ND, together with those after 29% compressive strain, are shown in Fig. 9a and 9b, respectively. Due to the limitation of sample size, we are not able to measure the texture of samples after tension.

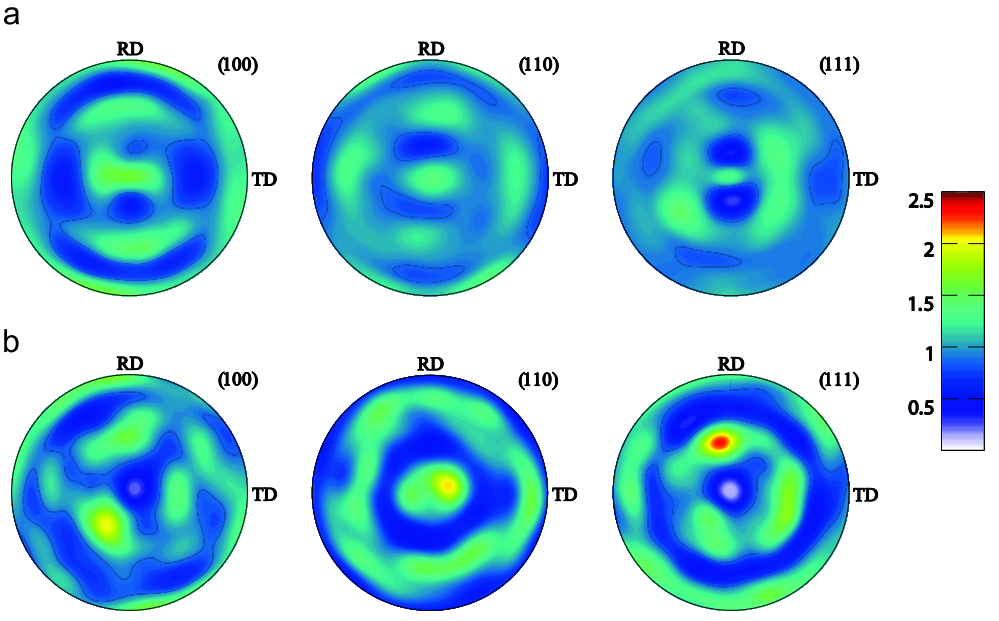

Fig. 9. Evolution of crystallographic texture for FeMnC from experiments while loading along the ND direction. (a) Initial texture. (b) Texture at 29% compressive strain, experiment.

Fig. 10 shows the stress–strain curves from FEM simulation when both dislocation slip and deformation twinning are activated, with Fig. 10a for tension and 10b for compression. Numerical predictions agree well with experimental results for the stress–strain responses in the ND direction. The texture evolutions from FEM simulations are shown in Fig. 10c and d, corresponding to texture at 52% tensile strain and 29% compressive strain, respectively. Texture at 29% compressive strain from our simulation also matches well with our experimental measurement shown in Fig. 9b. In particular, the primary (110) texture is captured nicely with the 300 initial orientations we used. We expect that even better match in stress–strain behavior and texture evolution can be achieved if systems with more representative grains can be simulated.

In Fig. 11a and b, we show the corresponding accumulative fractional strains as a function of the applied strain for tension and for compression in the ND direction, respectively. Similar to our observation when deformation is applied along the RD direction, deformation twinning has a smaller contribution to the overall plastic deformation when the macroscopic strain applied along the ND is greater than 20%. Corresponding equivalent plastic strain contour at 52% tensile strain and 29% compressive strain are shown, respectively, in Fig. 11c and d. While there exists a certain level inhomogeneous deformation, we do not see shear localization. Accompanying with the deformation inhomogeneity, we also observe strong stress fluctuation in individual grains, as seen from the average stress in typical grains shown in Fig. 8e (for tension) and 8f (for compression).

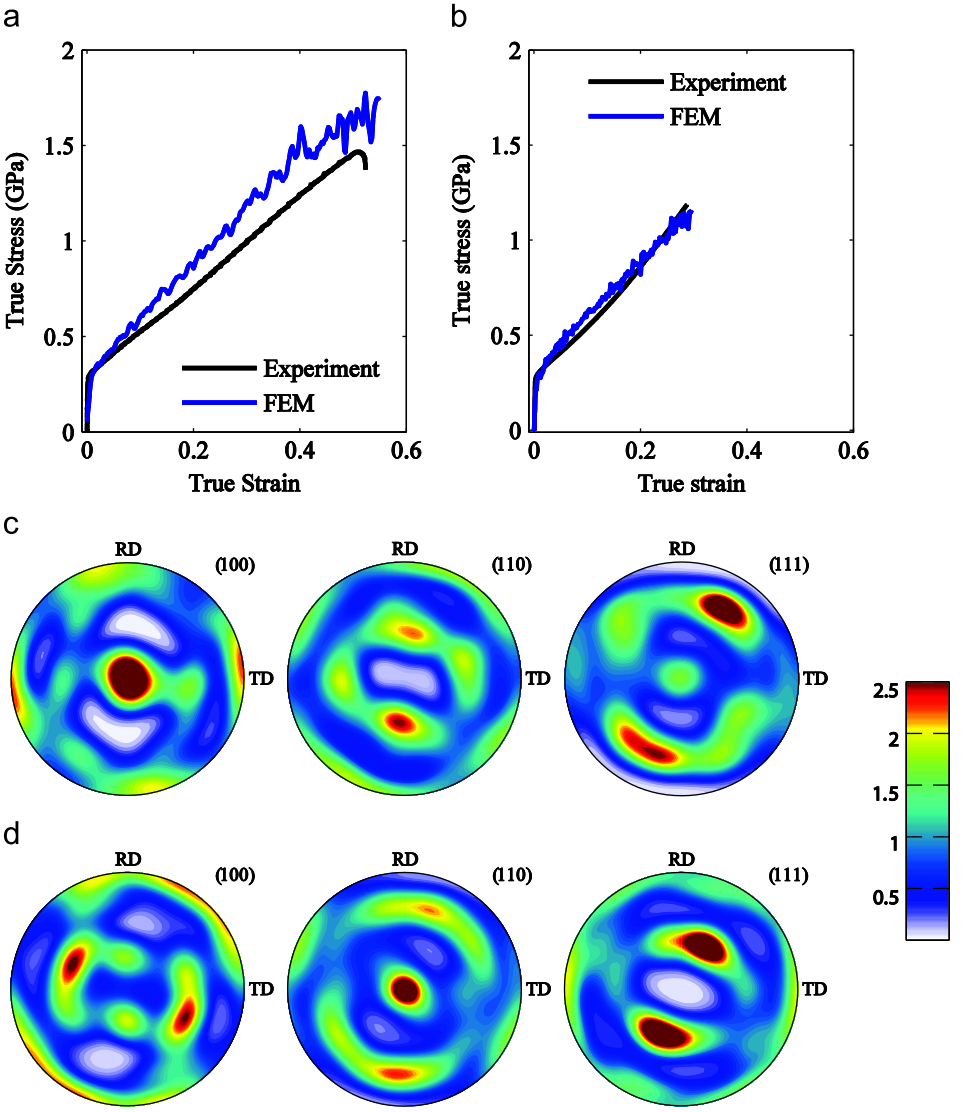

Fig. 10. Stress–strain curves and crystallographic texture for FeMnC when we apply loading along the ND direction. Both deformation twinning and dislocation slip are activated for plasticity. Stress–strain curves for (a) tension and (b) compression. (c) Texture at 52% tensile strain. (d) Texture at 29% compressive strain.

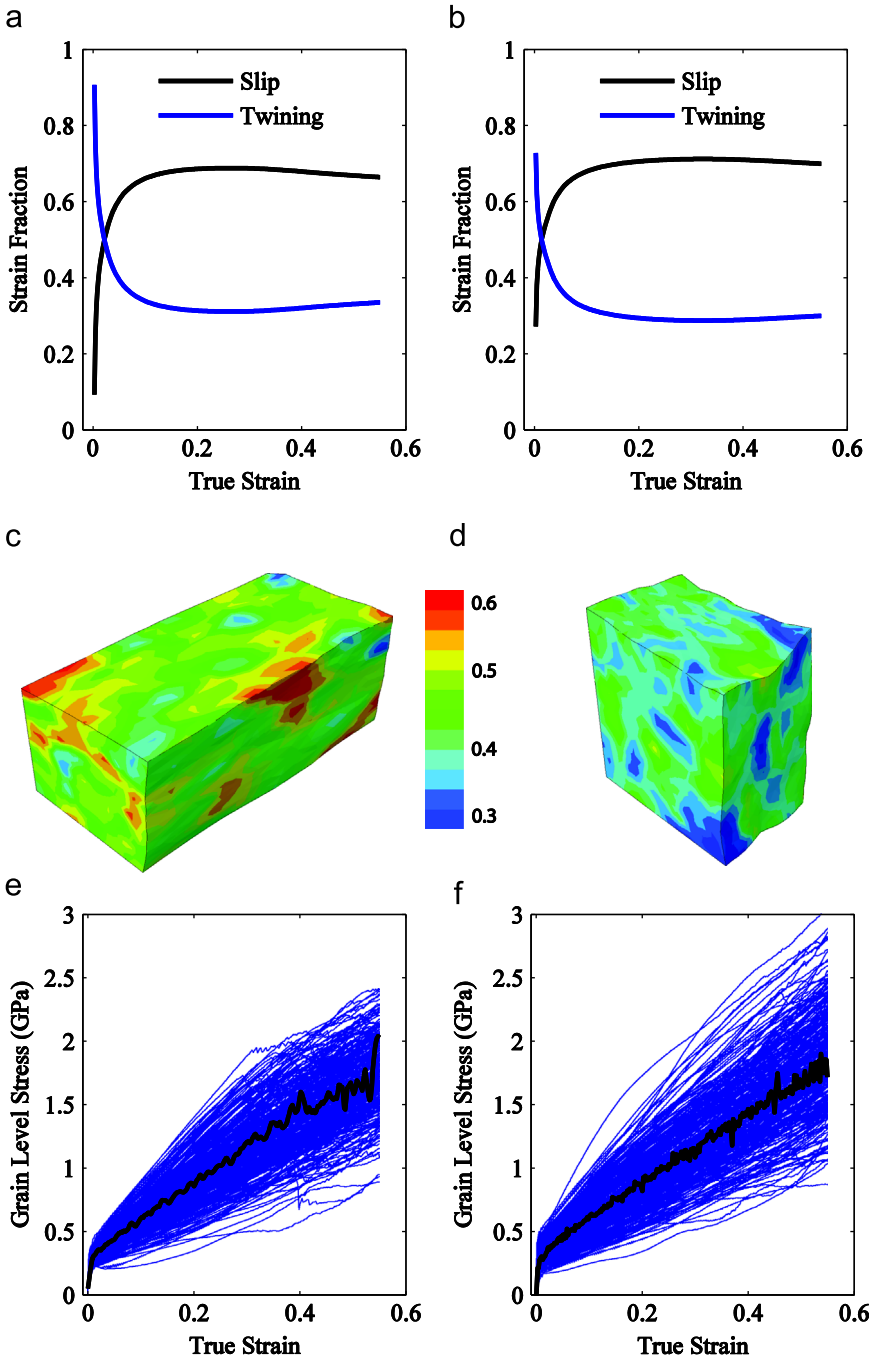

Fig. 11. Detailed grain level deformation from simulations while loading along the ND direction. (a) The fractional plastic strain contributed by individual mechanisms during tension. (b) Evolution of fractional plastic strain evolution during compression. Contours of equivalent plastic strain at (c) 52% tensile strain, and (d) at 29% compressive strain. Grain level stress as a function of strain during (e) tension and (f) compression. Blue lines are for average stresses along the loading axis for individual grains, and the black line is the macroscopic stress–strain response of the sample. (For interpretation of the references to color in this figure legend, the reader is referred to the web version of this article.)

6. Discussion and conclusion

In summary, we perform a systematic investigation on the strain hardening and texture evolution in high manganese TWIP steels, and develop a mechanistic model to explain the strain-hardening in crystals where deformation twinning dominates the plastic deformation. Using FeMnC TWIP steel, we show via both experimental measurements and finite-element simulations based on the classic crystal plasticity constitutive model, that deformation twinning plays a significant role for the strain hardening and texture evolution in TWIP steels. By including both deformation twinning and dislocation

slip, we obtain a good match between experimental measures and FEM simulations, for both stress–strain responses and texture evolution in TWIP steel during quasi-static deformation. While exploring the evolution of fractional strain with applied deformation, we find that twinning dominates the plastic deformation during the incipient of plasticity, and its fractional plastic strain reaches about 90% within 5% strain. The fractional strain by twinning drops quickly with straining while that by dislocation slip increases. Beyond 20% strain, both fractional strains seem to reach their steady state: dislocation slip occupies about 65% of the overall plastic strain, and deformation twinning takes about 35%. It indicates that even the materials are named as 'twinning induced plasticity steel'; more plastic deformation comes from dislocation slip over that contributed by twinning during the late stage of plasticity. This observation is consistent with analysis that concurrent activation of alternative yet competitive deformation mechanisms like dislocation slip and twinning in some FCC metals is probable (Barbier et al., 2012, 2009a, 2009b; Chin et al., 1969; Gutierrez-Urrutia et al., 2010; Meng et al., 2007; Wei, 2011b; Yang et al., 2006). We further testify the predictability of the FEM calculations by considering the mechanical response and texture evolution of the TWIP steel along the ND direction. The numerical modeling shows good predictability when both dislocation slip and deformation twinning are involved in plastic deformation.

Acknowledgments

The authors acknowledge support from MOST 973 of China (2012CB937500, 2011CB711103), National Natural Science Foundation of China (NSFC) (11021262), and the Chinese Academy of Sciences (KJCX2-EW-L03) for Y.W., and MOST 863 of China (Nr. 2012AA03A508) for Z.M. and D.T. Y.W. is very grateful to Prof. Huajian Gao and Dr. Xiaoyan Li for fruitful discussions on the strain hardening by deformation twinning.

References

Adler, P., Olson, G., Owen, W., 1986. Strain hardening of Hadfield manganese steel. Metall. Mater. Trans. A 17, 1725–1737.
Allain, S., 2002. Caracte′risation et mode′lisation thermome′caniques multi-e′chelles des me′canismes de de′formation et d'e′crouissage d'aciers auste′nitiques a'haute teneur en mangane'se-Application a'l'effet TWIP (Ph.D. thesis). INPL, Ecole des Mines de Nancy, France.
Allain, S., Bouaziz, O., Chateau, J.P., 2010. Thermally activated dislocation dynamics in austenitic FeMnC steels at low homologous temperature. Scr. Mater. 62, 500–503.
Allain, S., Chateau, J.P., Bouaziz, O., 2002. Constitutive model of the TWIP effect in a polycrystalline high manganese content austenitic steel. Steel Res. 73, 299–302.
Allain, S., Chateau, J.P., Bouaziz, O., 2004a. A physical model of the twinning-induced plasticity effect in a high manganese austenitic steel. Mater. Sci. Eng. A 387–389, 143–147.
Allain, S., Chateau, J.P., Bouaziz, O., Migot, S., Guelton, N., 2004b. Correlations between the calculated stacking fault energy and the plasticity mechanisms in Fe–Mn–C alloys. Mater. Sci. Eng. A 387–389, 158–162.
Allain, S., Chateau, J.P., Dahmoun, D., Bouaziz, O., 2004c. Modeling of mechanical twinning in a high manganese content austenitic steel. Mater. Sci. Eng. A 387–389, 272–276.
Allain, S., Cugy, P., Scott, C., Chateau, J.P., Rusinek, A., Deschamps, A., 2008. The influence of plastic instabilities on the mechanical properties of a high-manganese austenitic FeMnC steel. Int. J. Mater. Res. 99, 734–738.
Asaro, R.J., Krysl, P., Kad, B., 2003. Deformation mechanism transitions in nanoscale fcc metals. Philos. Mag. Lett. 83, 733–743.
Asaro, R.J., Needleman, A., 1985. Texture development and strain hardening in rate dependent polycrystals. Acta Metall. 33, 923–953.
Asaro, R.J., Suresh, S., 2005. Mechanistic models for the activation volume and rate sensitivity in metals with nanocrystalline grains and nano-scale twins. Acta Mater. 53, 3369–3382.
Barbier, D., Favier, V., Bolle, B., 2012. Modeling the deformation textures and microstructural evolutions of a Fe–Mn–C TWIP steel during tensile and shear testing. Mater. Sci. Eng. A 540, 212–225.
Barbier, D., Gey, N., Allain, S., Bozzolo, N., Humbert, M., 2009a. Analysis of the tensile behavior of a TWIP steel based on the texture and microstructure evolutions. Mater. Sci. Eng. A 500, 196–206.
Barbier, D., Gey, N., Bozzolo, N., Allain, S., Humbert, M., 2009b. EBSD for analysing the twinning microstructure in fine-grained TWIP steels and its influence on work hardening. J. Microsc. 235, 67–78.
Bayraktar, E., Khalid, F.A., Levaillant, C., 2004. Deformation and fracture behaviour of high manganese austenitic steel. J. Mater. Process. Technol. 147, 145–154.
Bouaziz, O., 2012. Strain-hardening of twinning-induced plasticity steels. Scr. Mater. 66, 982–985.
Bouaziz, O., Allain, S., Estrin, Y., 2010. Effect of pre-strain at elevated temperature on strain hardening of twinning-induced plasticity steels. Scr. Mater. 62, 713–715.
Bouaziz, O., Allain, S., Scott, C., 2008. Effect of grain and twin boundaries on the hardening mechanisms of twinning-induced plasticity steels. Scr. Mater. 58, 484–487.
Bouaziz, O., Allain, S., Scott, C.P., Cugy, P., Barbier, D., 2011a. High manganese austenitic twinning induced plasticity steels: a review of the microstructure properties relationships. Curr. Opin. Solid State Mater. Sci. 15, 141–168.
Bouaziz, O., Guelton, N., 2001. Modelling of TWIP effect on work-hardening. Mater. Sci. Eng. A 319–321, 246–249.
Bouaziz, O., Zurob, H., Chehab, B., Embury, J.D., Allain, S., Huang, M., 2011b. Effect of chemical composition on work hardening of Fe–Mn–C TWIP steels. Mater. Sci. Technol. 27, 707–709.
Brüx, U., Frommeyer, G., GrÄssel, O., Meyer, L.W., Weise, A., 2002. Development and characterization of high strength impact resistant Fe–Mn–(Al-, Si) TRIP/TWIP steels. Steel Res. 73, 294–298.
Bracke, L., Verbeken, K., Kestens, L., Penning, J., 2009. Microstructure and texture evolution during cold rolling and annealing of a high Mn TWIP steel. Acta Mater. 57, 1512–1524.
Chen, L., Kim, H.-S., Kim, S.-K., Cooman, B.C.D., 2007. Localized deformation due to Portevin–LeChatelier effect in 18Mn–0.6C TWIP austenitic steel. ISIJ Int. 47, 1804–1812.
Chin, G., Hosford, W., Mendorf, D., 1969. Accommodation of constrained deformation in fcc metals by slip and twinning. Proc. R. Soc. A 309, 433–456.
Christian, J.W., Mahajan, S., 1995. Deformation twinning. Prog. Mater. Sci. 39, 157.
Chung, K., Ahn, K., Yoo, D.-H., Chung, K.-H., Seo, M.-H., Park, S.-H., 2011. Formability of TWIP (twinning induced plasticity) automotive sheets. Int. J. Plast. 27, 52–81.

Cooman, B.C.D., Chin, K.-g., Kim, J., 2011. High Mn TWIP steels for automotive applications. In: Marcello Chiaberge (Ed.), New Trends and Developments in Automotive System Engineering. InTech, Croatia, pp. 101–128.
Cornette, D., Cugy, P., Hildenbrand, A., Bouzekri, M., Lovato, G., 2005. Ultra high strength FeMn TWIP steels for automotive safety parts.pdf. Rev. Métall. 12, 905–918.
Curtze, S., Kuokkala, V.T., 2010. Dependence of tensile deformation behavior of TWIP steels on stacking fault energy, temperature and strain rate. Acta Mater. 58, 5129–5141.
Curtze, S., Kuokkala, V.T., Oikari, A., Talonen, J., Hänninen, H., 2011. Thermodynamic modeling of the stacking fault energy of austenitic steels. Acta Mater. 59, 1068–1076.
Dancette, S., Delannay, L., Renard, K., Melchior, M.A., Jacques, P.J., 2012. Crystal plasticity modeling of texture development and hardening in TWIP steels. Acta Mater. 60, 2135–2145.
Dastur, Y.N., Leslie, W., 1981. Mechanism of work hardening in Hadfield manganese steel. Metall. Mater. Trans. A 12, 749–759.
Ding, H., Ding, H., Song, D., Tang, Z., Yang, P., 2011. Strain hardening behavior of a TRIP/TWIP steel with 18.8% Mn. Mater. Sci. Eng. A 528, 868–873.
Dumay, A., Chateau, J.P., Allain, S., Migot, S., Bouaziz, O., 2008. Influence of addition elements on the stacking-fault energy and mechanical properties of an austenitic Fe–Mn–C steel. Mater. Sci. Eng. A 483–484, 184–187.
Eshelby, J.D., 1957. The determination of the elastic field of an ellipsoidal inclusion, and related problems. Proc. R. Soc. A 241, 376–396.
Fernández, A., Pérez Prado, T., Wei, Y., Jérusalem, A., 2011. Continuum modeling of the response of a Mg alloy AZ31 rolled sheet during uniaxial deformation. Int. J. Plast. 27, 1739–1757.
Frommeyer, G., Brux, U., Neumann, P., 2003. Supra-ductile and high-strength manganese-TRIPTWIP steels for high energy absorption purposes. ISIJ Int. 43, 438–446.
Gebhardt, T., Music, D., Kossmann, D., Ekholm, M., Abrikosov, I.A., Vitos, L., Schneider, J.M., 2011. Elastic properties of fcc Fe–Mn–X (X=Al, Si) alloys studied by theory and experiment. Acta Mater. 59, 3145–3155.
Grässel, O., Krüger, L., Frommeyer, G., Meyer, L., 2000. High strength Fe–Mn–(Al, Si) TRIP/TWIP steels development-properties-application. Int. J. Plast. 16, 1391–1409.
Gutierrez-Urrutia, I., Zaefferer, S., Raabe, D., 2010. The effect of grain size and grain orientation on deformation twinning in a Fe–22 wt% Mn–0.6 wt% C TWIP steel. Mater. Sci. Eng. A 527, 3552–3560.
Huang, B.X., Wang, X.D., Rong, Y.H., Wang, L., Jin, L., 2006. Mechanical behavior and martensitic transformation of an Fe–Mn–Si–Al–Nb alloy. Mater. Sci. Eng. A 438–440, 306–311.
Idrissi, H., Renard, K., Ryelandt, L., Schryvers, D., Jacques, P.J., 2010a. On the mechanism of twin formation in Fe–Mn–C TWIP steels. Acta Mater. 58, 2464–2476.
Idrissi, H., Renard, K., Schryvers, D., Jacques, P.J., 2010b. On the relationship between the twin internal structure and the work-hardening rate of TWIP steels. Scr. Mater. 63, 961–964.
Idrissi, H., Ryelandt, L., Veron, M., Schryvers, D., Jacques, P.J., 2009. Is there a relationship between the stacking fault character and the activated mode of plasticity of Fe–Mn-based austenitic steels? Scr. Mater. 60, 941–944.
Jérusalem, A., Dao, M., Suresh, S., Radovitzky, R., 2008. Three-dimensional model of strength and ductility of polycrystalline copper containing nanoscale twins. Acta Mater. 56, 4647–4657.
Jeong, J.S., Woo, W., Oh, K.H., Kwon, S.K., Koo, Y.M., 2012. In situ neutron diffraction study of the microstructure and tensile deformation behavior in Al-added high manganese austenitic steels. Acta Mater. 60, 2290–2299.
Jin, J.E., Lee, Y.K., 2009. Strain hardening behavior of a Fe–18Mn–0.6C–1.5Al TWIP steel. Mater. Sci. Eng. A 527, 157–161.
Jin, J.E., Lee, Y.K., 2012. Effects of Al on microstructure and tensile properties of C-bearing high Mn TWIP steel. Acta Mater. 60, 1680–1688.
Kalidindi, S.R., Bronkhorst, C.A., Anand, L., 1992. Crystallographic texture evolution in bulk deformation processing of FCC metals. J. Mech. Phys. Solids 40, 537–569.
Karaman, I., Sehitoglu, H., Gall, K., Chumlyakov, Y.I., Maier, H.J., 2000. Deformation of single crystal Hadfield steel by twinning and slip. Acta Mater. 48, 1345–1359.
Kelly, A., Knowles, K.M., 2012. Crystallography and Crystal Defects. Longman, London.
Kim, J.-K., Chen, L., Kim, H.-S., Kim, S.-K., Estrin, Y., Cooman, B.C., 2009. On the tensile behavior of high-manganese twinning-induced plasticity steel. Metall. Mater. Trans. A 40, 3147–3158.
Kochmann, D.M., Le, K.C., 2009. A continuum model for initiation and evolution of deformation twinning. J. Mech. Phys. Solids 57, 987–1002.
Krauss, G., 1990. Steels: heat treatment and processing principles. ASM Int., 1–497.
Lü, Y., Hutchinson, B., Molodov, D.A., Gottstein, G., 2010. Effect of deformation and annealing on the formation and reversion of ε-martensite in an Fe–Mn–C alloy. Acta Mater. 58, 3079–3090.
Lü, Y., Molodov, D.A., Gottstein, G., 2011. Recrystallization kinetics and microstructure evolution during annealing of a cold-rolled Fe–Mn–C alloy. Acta Mater. 59, 3229–3243.
Lai, H., Wan, C., 1989. The study of work hardening in Fe–Mn–Al–C alloys. J. Mater. Sci. 24, 2449–2453.
Lee, T.-H., Shin, E., Oh, C.-S., Ha, H.-Y., Kim, S.-J., 2010. Correlation between stacking fault energy and deformation microstructure in high-interstitial-alloyed austenitic steels. Acta Mater. 58, 3173–3186.
Li, X.Y., Wei, Y.J., Lu, L., Lu, K., Gao, H.J., 2010. Dislocation nucleation governed softening and maximum strength in nano-twinned metals. Nature 464, 877–880.
Liang, X., McDermid, J.R., Bouaziz, O., Wang, X., Embury, J.D., Zurob, H.S., 2009. Microstructural evolution and strain hardening of Fe–24Mn and Fe–30Mn alloys during tensile deformation. Acta Mater. 57, 3978–3988.
Liu, Y., Wang, W.J., Xie, J.J., Sun, S.G., Wang, L., Qian, Y., Meng, Y., Wei, Y.J., 2012. Microstructure and mechanical properties of aluminum 5083 weldments by gas tungsten arc and gas metal arc welding. Mater. Sci. Eng. A 549, 7–13.
Lu, L., Chen, X.H., Huang, X., Lu, K., 2009. Revealing the maximum strength in nanotwinned copper. Science 323, 607–610.
Lu, L., Shen, Y.F., Chen, X.H., Qian, L.H., Lu, K., 2004. Ultrahigh strength and high electrical conductivity in copper. Science 304, 422–426.
Mahajan, S., Chin, G., 1973. Formation of deformation twins in fcc crystals. Acta Metall. 21, 1353–1363.
Meng, L., Yang, P., Xie, Q., Ding, H., Tang, Z., 2007. Dependence of deformation twinning on grain orientation in compressed high manganese steels. Scr. Mater. 56, 931–934.
Meyers, M., Vöhringer, O., Lubarda, V., 2001. The onset of twinning in metals: a constitutive description. Acta Mater. 49, 4025–4039.
Mi, Z., Tang, D., Yan, L., Guo, J., 2005. High-strength and high-plasticity TWIP steel for modern vehicle. J. Mater. Sci. Technol. 21, 451–454.
Mi, Z., Tang, D., Zhao, A., Jiang, H., 2012. Microstructure evolution during deformation process and mechanical characteristics of a Fe–Mn–C TWIP steel. Steel Res. 83, 346–351.
Park, K.-T., Jin, K.G., Han, S.H., Hwang, S.W., Choi, K., Lee, C.S., 2010. Stacking fault energy and plastic deformation of fully austenitic high manganese steels: effect of Al addition. Mater. Sci. Eng. A 527, 3651–3661.
Pitteri, M., 1985. On $\nu+1$-lattices. J. Elast. 15, 3–25.
Pitteri, M., 1986. On type-2 twins in crystals. Int. J. Plast. 2, 99–106.
Proust, G., Tomé, C.N., Kaschner, G.C., 2007. Modeling texture, twinning and hardening evolution during deformation of hexagonal materials. Acta Mater. 55, 2137–2148.
Raghavan, K., Sastri, A., Marcinkowski, M., 1969. Nature of the work-hardening behavior in Hadfields manganese steel. Trans. AIME 245, 1569–1575.
Roters, F., Eisenlohr, P., Hantcherli, L., Tjahjanto, D.D., Bieler, T.R., Raabe, D., 2010. Overview of constitutive laws, kinematics, homogenization and multiscale methods in crystal plasticity finite-element modeling: theory, experiments, applications. Acta Mater. 58, 1152–1211.

Saeed-Akbari, A., Mosecker, L., Schwedt, A., Bleck, W., 2011. Characterization and prediction of flow behavior in high-manganese twinning induced plasticity steels: part I. Mechanism maps and work-hardening behavior. Metall. Mater. Trans. A 43, 1688–1704.
Saleh, A.A., Pereloma, E.V., Gazder, A.A., 2011. Texture evolution of cold rolled and annealed Fe–24Mn–3Al–2Si–1Ni–0.06C TWIP steel. Mater. Sci. Eng. A 528, 4537–4549.
Sato, K., Ichinose, M., Hirotsu, Y., Inoue, Y., 1989. Effects of deformation induced phase transformation and twinning on the mechanical properties of austenitic Fe–Mn–Al alloys. ISIJ Int. 29, 868–877.
Scott, C., Allain, S., Guelton, N., Arcelor, F., 2006. The development of a new Fe–Mn–C austenitic steel for automotive applications. Rev. Métall. 103, 293–302.
Sevillano, J.G., 2009. An alternative model for the strain hardening of FCC alloys that twin, validated for twinning-induced plasticity steel. Scr. Mater. 60, 336–339.
Shiekhelsouk, M., Favier, V., Inal, K., Cherkaoui, M., 2009. Modelling the behaviour of polycrystalline austenitic steel with twinning-induced plasticity effect. Int. J. Plast. 25, 105–133.
Staroselsky, A., Anand, L., 1998. Inelastic deformation of polycrystalline face centered cubic materials by slip and twinning. J. Mech. Phys. Solids 46 (671–673), 675–696.
Staroselsky, A.V., 1998. Crystal Plasticity due to Slip and Twinning (Ph.D. thesis). Massachusetts Institute of Technology, USA.
Vercammen, S., 2004. Processing and Tensile Behaviour of TWIP Steels Microstructural and Texture Analysis (Ph. D. thesis). Katholieke Universiteit Leuven, Belgium.
Vercammen, S., Blanpain, B., De Cooman, B.C., Wollants, P., 2004. Cold rolling behaviour of an austenitic Fe–30Mn–3Al–3Si TWIP-steel: the importance of deformation twinning. Acta Mater. 52, 2005–2012.
Wang, X., Zurob, H., Embury, J., Ren, X., Yakubtsov, I., 2010. Microstructural features controlling the deformation and recrystallization behaviour Fe–30% Mn and Fe–30% Mn–0.5% C. Mater. Sci. Eng. A 527, 3785–3791.
Wei, Y.J., 2011a. The kinetics and energetics of dislocation mediated de-twinning in nano-twinned face-centered cubic metals. Mater. Sci. Eng. A 528, 1558–1566.
Wei, Y.J., 2011b. Scaling of maximum strength with grain size in nanotwinned fcc metals. Phys. Rev. B 83. 132104-1.
Wei, Y.J., Anand, L., 2007. A constitutive model for powder-processed nanocrystalline metals. Acta Mater. 55, 921–931.
Wei, Y.J., Su, C., Anand, L., 2006. A computational study of the mechanical behavior of nanocrystalline fcc metals. Acta Mater. 54, 3177–3190.
Yang, P., Xie, Q., Meng, L., Ding, H., Tang, Z., 2006. Dependence of deformation twinning on grain orientation in a high manganese steel. Scr. Mater. 55, 629–631.
Yoo, J.D., Hwang, S.W., Park, K.-T., 2009. Factors influencing the tensile behavior of a Fe–28Mn–9Al–0.8C steel. Mater. Sci. Eng. A 508, 234–240.
Yoo, J.D., Park, K.-T., 2008. Microband-induced plasticity in a high Mn–Al–C light steel. Mater. Sci. Eng. A 496, 417–424.
Zavattieri, P.D., Savic, V., Hector Jr., L.G., Fekete, J.R., Tong, W., Xuan, Y., 2009. Spatio-temporal characteristics of the Portevin–Le Châtelier effect in austenitic steel with twinning induced plasticity. Int. J. Plast. 25, 2298–2330.
Zhu, B., Asaro, R.J., Krysl, P., Bailey, R., 2005. Transition of deformation mechanisms and its connection to grain size distribution in nanocrystalline metals. Acta Mater. 53, 4825–4838.